Gastroenterology 2025;168:508–524

Creeping Fat–Derived Free Fatty Acids Induce Hyperplasia of Intestinal Muscularis Propria Muscle Cells: A Novel Link Between Fat and Intestinal Stricture Formation in Crohn's Disease

Weiwei Liu,[1] Ren Mao,[1,2] Thi Hong Nga Le,[1] Gail West,[1] Venkateshwari Varadharajan,[3] Rakhee Banerjee,[3] Genevieve Doyon,[1] Pranab Mukherjee,[1] Quang Tam Nguyen,[1] Anny Mulya,[1] Julie H. Rennison,[3] Ilyssa O. Gordon,[4] Michael Cruise,[4] Shaomin Hu,[4] Doug Czarnecki,[1] Thomas Plesec,[4] Jyotsna Chandra,[1] Suhanti Banerjee,[1] Jie Wang,[1,5] William J. Massey,[1] Idan Goren,[1] Si-Nan Lin,[1] Satya Kurada,[6] Benjamin L. Cohen,[7] Taha Qazi,[7] Stefan D. Holubar,[8] Jeremy Lipman,[8] Arielle Kanters,[8] Christy M. Gliniak,[9] Philipp E. Scherer,[9] Min-Hu Chen,[2] Britta Siegmund,[10] Andrei I. Ivanov,[1] Claudio Fiocchi,[1,7] David R. Van Wagoner,[3] J. Mark Brown,[3] and Florian Rieder[1,7,11]

[1]Department of Inflammation and Immunity, Lerner Research Institute, Cleveland Clinic Foundation, Cleveland, Ohio; [2]Department of Gastroenterology, First Affiliated Hospital of Sun Yat-sen University, Guangzhou, China; [3]Department of Cardiovascular and Metabolic Sciences, Lerner Research Institute, Cleveland Clinic, Cleveland, Ohio; [4]Department of Pathology, Robert J. Tomsich Pathology and Laboratory Medicine Institute, Cleveland Clinic Foundation, Cleveland, Ohio; [5]Xinxiang Key Laboratory of Inflammation and Immunology, Xinxiang Medical University, Xinxiang, China; [6]Division of Gastroenterology and Hepatology, Indiana University School of Medicine, Indianapolis, Indiana; [7]Department of Gastroenterology, Hepatology and Nutrition, Digestive Diseases Institute, Cleveland Clinic Foundation, Cleveland, Ohio; [8]Department of Colorectal Surgery, Digestive Diseases Institute, Cleveland Clinic Foundation, Cleveland, Ohio; [9]Touchstone Diabetes Center, The University of Texas Southwestern Medical Center at Dallas, Dallas, Texas; [10]Charité Universitätsmedizin Berlin, corporate member of Freie Universität Berlin and Humboldt-Universität zu Berlin, Department of Gastroenterology, Infectious Diseases and Rheumatology, Berlin, Germany; and [11]Cleveland Clinic Program for Global Translational Inflammatory Bowel Diseases

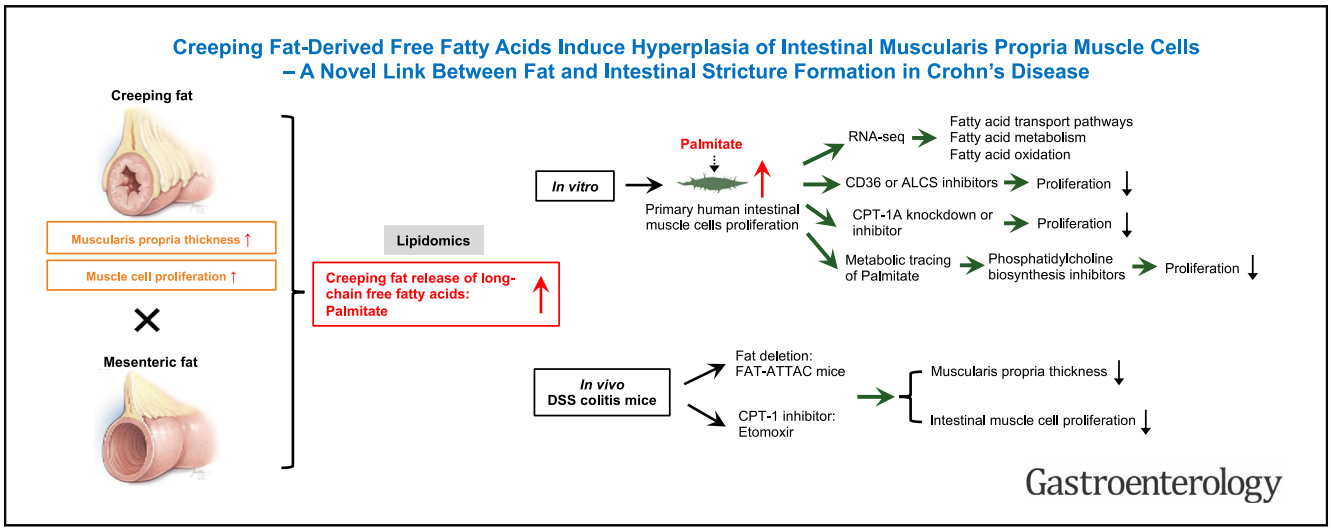

See editorial on page 454.

BACKGROUND & AIMS: In Crohn's disease, wrapping of mesenteric fat around the bowel wall, so-called "creeping fat," is highly associated with strictures. The strongest contributor to luminal narrowing in strictures is a thickening of the human intestinal muscularis propria (MP). We investigated creeping fat–derived factors and their effect on mechanisms of human intestinal MP smooth muscle cell (HIMC) hyperplasia. **METHODS:** Free fatty acids (FFAs) in creeping fat or non-creeping mesenteric fat organ cultures were measured via lipidomic mass spectrometry. Primary HIMCs were exposed to FFAs and cell proliferation was assessed. Intracellular FFA metabolism pathways and reactive oxygen species were functionally evaluated. Muscle thickness was investigated in dextran sodium sulfate colitis with small molecule inhibition of FFA transport and a novel fat deletion mouse model. **RESULTS:**

Subserosal creeping fat is associated with a markedly thickened MP. Experimental deletion of mesenteric fat (FAT-ATTAC [fat apoptosis through targeted activation of caspase 8] mouse) reduced MP thickness. Human creeping fat–conditioned medium strongly up-regulated HIMC proliferation. Creeping fat released higher amounts of 5 long-chain FFAs, including palmitate. Inhibition of HIMC long-chain FFA metabolism or FFA uptake into mitochondria through carnitine palmitoyltransferase-1 reduced the palmitate-induced HIMC proliferation. Blockade of conversion of palmitate into phospholipids reduced HIMC proliferation. Prophylactic inhibition of carnitine palmitoyltransferase-1 in experimental dextran sodium sulfate colitis did not ameliorate inflammation, but reduced MP thickness. **CONCLUSIONS:** Creeping fat–released long-chain FFAs induce a selective proliferative response by HIMC. These results point to creeping fat as a novel contributor to stricture formation in Crohn's disease.

Keywords: Fibrostenosis; Anti-Fibrotic Therapy; Hypertrophy; Hyperplasia; Lipidomics.

WHAT YOU NEED TO KNOW

BACKGROUND AND CONTEXT

In Crohn's disease (CD), creeping fat is highly associated with strictures. The strongest contributor to luminal narrowing in strictures is thickening of the human intestinal muscularis propria. We investigated creeping fat–derived factors and their effect on intestinal muscularis propria smooth muscle cell hyperplasia.

NEW FINDINGS

Long-chain free fatty acids released by creeping fat induced smooth muscle cell proliferation. This occurs through uptake of fatty acids into mitochondria and their oxidation, as well as through lipid metabolism. This is targetable through inhibition of the mitochondrial transporter carnitine palmitoyl transferase 1.

LIMITATIONS

Our surgical cohort represents late and already established disease. We are not able to elucidate a link of medications at time of surgery with the findings.

CLINICAL RESEARCH RELEVANCE

An increasing understanding of stricturing CD, a complication for which no selective therapies exist, can lead to development of novel anti-stricture treatments. Blockade of carnitine palmitoyl transferase 1 may be tested in clinical trials for stricturing CD and would, for the first time, target the muscle thickening and not the deposition of extracellular matrix.

BASIC RESEARCH RELEVANCE

These results provide a new resource for a better understanding of CD stricture formation. The scientific community and industry can use this information to develop novel therapeutic drug targets. This work, for the first time, mechanistically links creeping fat with muscle hyperplasia in stricturing CD.

The majority of patients with Crohn's disease (CD) develop symptomatic intestinal strictures, which comprise a major indication for surgery.[1] Currently, there are no specific anti-stricture therapies available, despite our increasing understanding of bowel fibrogenesis, including intestinal fibroblast activation and extracellular matrix (ECM) deposition secondary to mucosal inflammation.[1–3] Recently, intestinal muscularis propria (MP) smooth muscle hyperplasia, but not ECM deposition, was identified as a major contributor to luminal narrowing in stricturing CD.[4] Targeting intestinal smooth muscle hyperplasia may be an important strategy to treat CD-associated strictures.

Mesenteric fat wrapping around the inflamed gut, also known as "creeping fat," is pathognomonic of CD.[5,6] Evidence suggests that creeping fat is associated with transmural inflammation, MP hyperplasia, excessive ECM deposition, and stricture formation in CD.[7] The close proximity of creeping fat and the MP makes an interaction between them likely. We previously established a functional interaction between activated human intestinal MP smooth muscle cells (HIMCs) and creeping fat, as well as non-creeping mesenteric fat.[3] HIMC-derived fibronectin led to pre-adipocyte migration via integrin-mediated mechanisms, potentially leading to creeping fat formation.[3] However, the interaction of human creeping fat–derived mediators contributing to MP hyperplasia has never been investigated.

In the present study, we carefully evaluated factors released by creeping fat and affecting HIMCs using primary human cells, lipidomics, RNA sequencing, cell–cell interaction, and murine chemical and transgenic models. The results suggest a sequential series of events where subserosal creeping fat releases long-chain free fatty acids (FFAs), including palmitate, which induce a proliferative response by HIMCs. The palmitate effect on HIMC proliferation was dependent on uptake into HIMCs and the long-chain fatty acid (FA) transporter carnitine palmitoyltransferase (CPT) 1A. Palmitate in HIMCs is converted into phospholipids (PLs) and inhibition of their metabolism reduced palmitate-induced HIMC proliferation. Inhibition of CPT-1 or deletion of fat in vivo reduced MP thickness in murine colitis models. These results point to creeping fat as a novel contributor to stricture formation in CD.

Materials and Methods

Procurement and Histopathology of Human Intestinal Tissues

Full-thickness, freshly resected, intestinal specimens from subjects with CD and controls, comprising ulcerative colitis

Abbreviations used in this paper: **CD, Crohn's disease; CDns, Crohn's disease nonstrictured; CDs, Crohn's disease strictured; CPT, carnitine palmitoyltransferase; DSS, dextran sodium sulfate; ECM, extracellular matrix; FAT-ATTAC, fat apoptosis through targeted activation of caspase 8; FFA, free fatty acid; HIMC, human intestinal muscle cell; MP, muscularis propria; NL, normal; PC, phosphatidyl choline; PL, phospholipid; ROS, reactive oxygen species; UC, ulcerative colitis; WT, wild-type.**

Most current article

0016-5085/$36.00
https://doi.org/10.1053/j.gastro.2024.10.034

SMALL BOWEL

(UC), diverticular disease, and apparently healthy tissue (ie, constipation and healthy margin of resections from patients with colorectal cancer; termed "normal" [NL]) were procured as described previously.[2,8–11] CD specimens were classified based on gross anatomy into strictured (CDs) and non-strictured (CDns). Fat was classified into creeping fat or non-creeping mesenteric fat. Creeping fat, as opposed to noncreeping mesenteric fat, was defined by the presence of broad-based fat tissue on the anti-mesenteric serosal aspect of the resected intestine on gross examination[3,12] or, in case the anti-mesenteric serosal side was not available on the resection specimen, creeping fat was defined by its aspect of obliteration or loss of the bowel-mesenteric angle. In our cohort of surgical resection specimens, creeping fat was linked to stricturing disease in all cases, and no creeping fat without strictures was observed. Creeping fat and noncreeping mesenteric fat can be considered part of the same mesenteric continuum. Hence the term *mesenteric fat*, which is used throughout this article for clarity, also encompasses "noncreeping mesenteric fat." CD resections were all derived from the small bowel. This procurement system was validated by means of histopathologic evaluation performed by a trained inflammatory bowel disease pathologist.[2,3,8] Representative histopathologic sections to include the zone over which creeping fat or noncreeping mesenteric fat integrates with the adjoining MP were obtained, formalin-fixed, and embedded in paraffin.[3] Five-micrometer sections were prepared and slides were stained with hematoxylin and eosin and Masson trichrome by the standard methods used in the Anatomic Pathology Department of the Cleveland Clinic.

Measurement of Thickness of the Muscularis Propria

The thickness of the MP on histopathologic specimen was measured as reported previously. Briefly, thickness of MP was determined on hematoxylin and eosin slides with a DP2-SAL digital camera (Olympus, Tokyo, Japan). Thickness of the MP was measured separately for the inner and outer layer of the MP by observers blinded to the diagnosis, and for each layer 3 measurements were performed and averaged per specimen. Measurements were confirmed by an independent second observer, as reported previously.[3]

Experimental Dextran Sodium Sulfate–Induced Colitis

Dextran sodium sulfate model with genetic deletion of fat. C57BL/6J FAT-ATTAC (fat apoptosis through targeted activation of caspase 8) mice were generated and kindly provided by Dr Philipp Scherer, University of Texas Southwestern.[13] Within 2 weeks of administration of the dimerizer AP20187 (FK1012 analog), FAT-ATTAC mice showed ablation of adipose tissue, without significant secondary effects in other tissues.[13] Adipocyte progenitors are not affected. This is crucial, as it allows the selective assessment of the effect of fat-derived mediators at the interface of MP and mesenteric fat. Six- to 8-week-old FAT-ATTAC mice and wild-type (WT) littermates were subjected to administration of dimerizer AP20187 (0.25 mg/kg body weight of mice, intraperitoneal injection; Takara, San Jose, CA) or vehicle (0.4% ETOH, 10% polyethylene glycol 400, and 89.6% phosphate-buffered saline) twice per week throughout the experiment. After 2 weeks of injections (4 injections) and before starting induction of colitis, efficacy of fat deletion was confirmed by measuring whole-body fat mass using echo magnetic resonance tomography (EchoMRI-100H System; EchoMRI LLC, Houston, TX). Colitis was induced by 1.5% dextran sodium sulfate (DSS; 35–50,000 kDa; MP Biomedicals, Santa Ana, CA) in the drinking water for 7 days.

Dextran sodium sulfate model with administration of the carnitine palmitoyl transferase inhibitor etomoxir. Six- to 8-week-old Balb/c WT mice were subjected to daily administration of etomoxir (60 mg/kg body weight of mice, intraperitoneal injection, MedChemExpress, Monmouth Junction, NJ) or vehicle (10% dimethyl sulfoxide, 10% ETOH, 40% polyethylene glycol 400, and 40% phosphate-buffered saline) the day before 3.5% DSS administration (MP Biomedicals, Santa Ana, CA) in the drinking water for 7 days and all throughout the experiment.

The respective DSS doses were chosen after separate dose titration experiments in the above-mentioned mouse strains. Experimental colitis was performed in at least 2 separate experiments. All mice per group were age-matched, sex-matched, and were co-housed as derived from the same litter and per genotype to minimize influence from differences in microbial flora composition.[14] Clinical disease activity was determined every other day by measuring body weight loss, stool consistency, and presence of occult or overt blood in the stools, as described previously.[2,8,11] At the end of the experiment, animals were euthanized by CO_2 asphyxiation, followed by cervical dislocation. The entire colon was removed, cleaned, and measured from the ileocecal junction to the anus. Histology was performed on paraffin-embedded, 3-μm-thick transverse sections stained with hematoxylin and eosin, Masson trichrome, or specific antibodies. Slides were scored by experienced pathologists (I.O.G., S.H.) blinded to the experimental groups using 1 score separately for inflammation and fibrosis.[2,8,11] The thickness of the MP was calculated on well-oriented colon cross sections. Observers blinded to the treatment groups measured the MP thickness underlying fat (mesenteric side) or not underlying fat (anti-mesenteric side) separately with 2 measurements averaged per MP region using QuPath software.[15]

Immunostaining, organ culture of mesenteric fat, and collection of fat-conditioned medium can be found in the Supplementary Materials.

Lipidomics of noncreeping mesenteric fat and creeping fat conditioned medium. Conditioned medium of noncreeping mesenteric fat and creeping fat were processed for lipidomics and analyzed as reported previously.[16] Briefly, samples were directly transesterified into FA methyl esters by heating samples with sulfuric acid in excess methanol. The resulting FA methyl esters were extracted with petroleum ether, concentrated with a stream of nitrogen and then analyzed by gas chromatography. FA methyl ester samples were injected into a Shimadzu 2010 gas chromatograph (Shimadzu, Kawasaki City, Japan), separating 30 FAs ranging from 12 carbons to 24 carbons. FAs were identified by comparison with authentic standards (NuChek Prep, Elysian MN). FAs were quantified by inclusion of an odd chain internal standard (NuChek Prep).

FFA assay quantification kit, isolation and culture of primary human intestinal cells, preparation of FAs, quantitative reverse transcriptase polymerase chain reaction, proliferation

assays, small interfering RNA transfection of HIMCs, immunoblotting, measurement of cellular reactive oxygen species (ROS), measurement of FA esterification and de novo lipogenesis rates in HIMCs, lipidomic profiling of PLs in HIMCs after exposure to palmitate, additional reagents and antibodies, and statistical analysis can be found in Supplementary Materials.

Results

Creeping Fat Is Associated With Thickening of the Muscularis Propria in Crohn's Disease

To explore the hypothesis that MP with noncreeping mesenteric fat or creeping fat interactions could lead to thickening of the muscle and intestinal stricture with obstruction, we first investigated the anatomic association of creeping fat and intestinal strictures on gross histopathology (Figure 1*A*). Creeping fat wrapping around CD small bowel segments was associated with luminal narrowing, which is consistent with previous studies.[17] In fact, all our surgical resections for CD strictures exhibited creeping fat. Upon histopathologic examination (Figure 1*B*), creeping fat was positioned underneath the serosal layer and, of relevance to this investigation, in direct contact with the MP (see Supplementary Figure 1*A* to further illustrate this spatial relationship). Strikingly, MP interna, externa, or total MP underlying creeping fat in CDs was markedly thicker compared with MP underlying noncreeping mesenteric fat in NL, UC, and CDns (Figure 1*C*, Supplementary Figure 1*B*; associated clinical data of tissues used for histopathology in this article are in Supplementary Table 2). A robustly increased number of Ki67 (proliferation marker)-positive cells in the MP of CDs tissue underlying creeping fat was noted compared with the MP of CDns, UC, and NL tissues underlying noncreeping mesenteric fat (Figure 1*D*; additional representative images are in Supplementary Figure 1*C*). A marked amount of Ki67-positive proliferating cells were also positive for the smooth muscle marker desmin, suggesting those are MP smooth muscle cells (Figure 1*E* and *F*). This demonstrates an association of the presence of creeping fat with MP proliferation and thickening.

Genetic Deletion of Fat Reduces Muscularis Propria Thickness in Dextran Sodium Sulfate Colitis

To assess the principle of fat interacting with the MP, we generated the so-called "FAT-ATTAC" mouse, in which administration of the dimerizer AP20187 activates caspase-8, deleting adipocytes through apoptosis.[13] EchoMRI analysis and macroscopic observation confirmed a robust 70% reduction in the body fat mass and reduction in abdominal fat, respectively, in FAT-ATTAC mice compared with baseline within 2 weeks (Figure 2*A* and *B*). We next exposed FAT-ATTAC mice or WT controls, pretreated for 2 weeks with dimerizer, to DSS for 7 days to induce colitis (Figure 2*C*). There was no clinically meaningful or significant difference in weight loss, clinical colitis score, clinical colitis subscores, or colon length changes in the DSS-treated animals throughout the experiment (Figure 2*D* and Supplementary Figures 2*A*–*C*). Histopathologic evaluation of the intestinal segments revealed mesenteric fat tissue atrophy in the dimerizer-treated animals (Figure 2*E*). The degree of inflammation or fibrosis increased in DSS-treated compared with no-DSS animals. No difference was observed when comparing DSS WT and DSS FAT-ATTC dimerizer-treated mice (Figure 2*F* and *G*), indicating no effect of fat deletion on inflammation or fibrosis. Of relevance, in WT mice with DSS treatment, the MP underlying the mesentery thickened. Dimerizer-treated FAT-ATTAC mice did not show any increase in MP thickening (Figure 2*H*, Supplementary Figure 2*D*). Concordant with these findings, DSS-treated WT animals showed an increase in proportion of $Ki67^+$ cells in the intestinal MP underlying the mesentery, which was reduced in the FAT-ATTAC dimerizer-treated DSS mice (Figure 2*I*). Most of the Ki67-positive cells also stained positive for desmin, indicating they are smooth muscle cells (Figure 2*J*). DSS-treated animals showed an increase in colonic inflammatory (*Il1b, Il6*, and *Tnf*) and ECM (*Fn1, Col1a1,* and *Col3a1*) gene expression, in the intestinal wall, regardless of FAT-ATTAC or WT background (Figure 2*K*). This suggests that presence of mesenteric fat is required for MP thickening in experimental colitis, but absence of mesenteric fat does not influence inflammation or fibrosis in the intestinal wall.

Creeping Fat–Derived Free Fatty Acids Induce Proliferation of Human Intestinal Muscularis Propria Cells

To provide evidence that creeping fat is functionally involved in HIMC proliferation, we generated conditioned medium from human NL, UC, and CD noncreeping mesenteric and creeping fat for use in HIMC proliferation (Figure 3*A*). We purposefully chose this approach to capture actively secreted or released mediators rather than using whole tissue lysates that may contain intracellular contents mixed with secreted or released components. Creeping fat–conditioned medium had the strongest effect on HIMC proliferation compared with noncreeping mesenteric fat–conditioned medium from CDns, UC, or NL (Figure 3*B*). There was no difference in HIMC proliferation when comparing noncreeping mesenteric fat–conditioned medium from CDns, UC, or NL. Adipocytes—the major cell type in creeping fat—contain rich lipid droplets, suggesting that lipids, such as FFAs, may be responsible for the observed changes.[6] Conditioned medium from creeping fat revealed increased concentrations of FFAs compared with CDns, UC, and NL noncreeping mesenteric fat–conditioned medium (Supplementary Figure 3*A*). Using unbiased lipidomics, principal component analysis separated creeping fat from CDns, UC, and NL noncreeping mesenteric fat–conditioned medium (Supplementary Figure 3*B*). The long-chain FFAs myristic acid (14:0), pentadecanoic (pentadecylic) acid (15:0), palmitate (16:0), palmitoleic acid (16:1), oleic acid (18:1), linoleic acid (18:2), γ-linolenic acid (16:3 ω-6), and α-linolenic acid (16:3 ω-3) were significantly elevated in creeping fat compared with controls, with palmitate

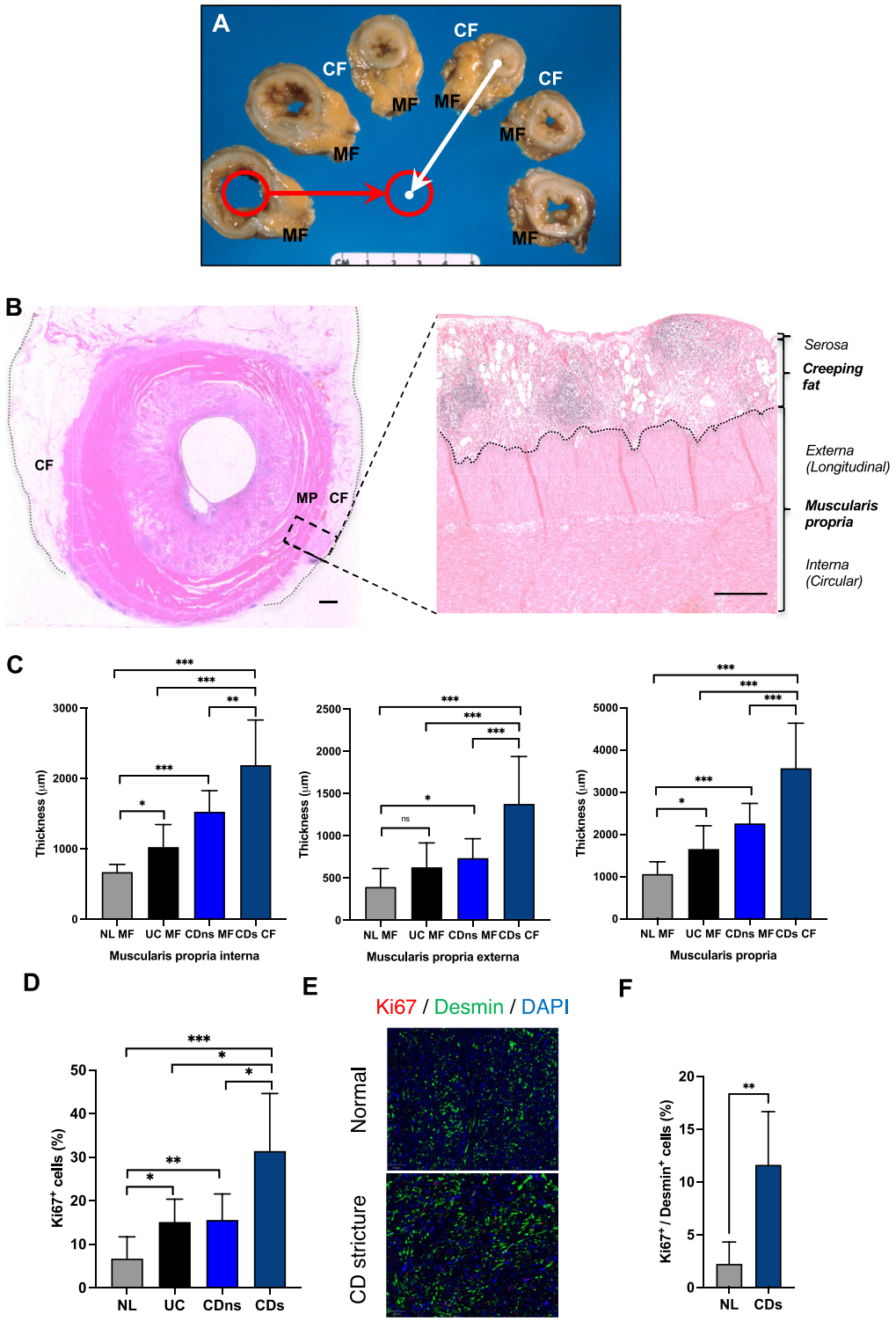

Figure 1. Association between creeping fat (CF), intestinal stricture, and MP thickness. (*A*) Gross pathology of intestinal resection tissue rings, cut along the length of an intestinal stricture. *Red line* indicates the healthy lumen proximal to the stricture. *White line* indicates the area of maximal luminal narrowing. CF is surrounding the intestinal stricture. (*B*) Hematoxylin and eosin staining of an intestinal stricture resection. CF (marked by *gray dotted line* on *left*) is interposed between the serosa and MP. The *black dotted line* marks the zone between CF and MP. *Scale bars:* 1000 μm. (*C*) The MP interna, externa, and total thickness in CD resection tissues are significantly increased in the MP underlying CF in CDs compared with the MP underlying noncreeping mesenteric fat (MF) in CDns, UC, and NL. n = 7–21 per group. (*D*) The proportion of Ki67$^+$ cells is higher in CDs compared with all other groups. (*E*) Representative immunofluorescence stainings of the human MP with a selective antibody to Ki67 (*red*), desmin (*green*), and 4′,6-diamidino-2-phenylindole (DAPI) (*blue*) in the external MP of NL and CDs are shown. *Scale bar:* 50 μm. (*F*) The proportion of Ki67$^+$/desmin$^+$ is increased in CDs compared with NL with desmin$^+$ cells comprising a marked proportion of Ki67$^+$ cells. n = 6–8 per group. Data are presented as mean ± SEM. **P* < .05; ***P* < .01; ****P* < .001.

showing the highest-fold increase (Figure 3*C*, Supplementary Tables 3 and 4). The FFAs myristic acid, pentadecanoic acid, palmitate, palmitoleic acid, and oleic acid markedly induced proliferation of HIMCs, with palmitate and oleic acid showing the strongest effect (Figure 3*D*). Due to the robust release of palmitate by creeping fat and its prominent effect on HIMC proliferation, we used palmitate for further experiments. palmitate's effect on proliferation was dose-dependent, with 50-μM concentration achieving the highest induction of proliferation (Supplementary

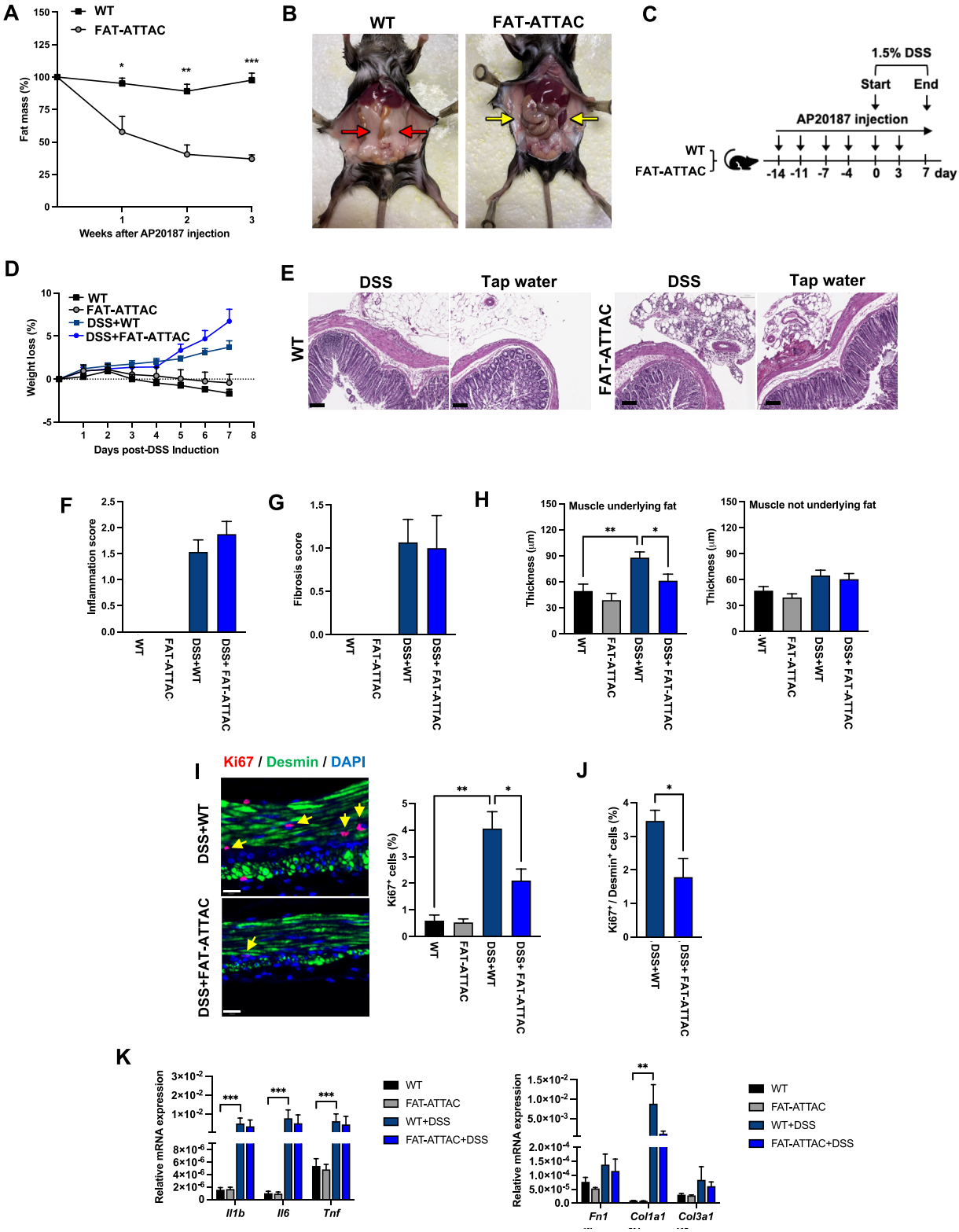

Figure 3*C*). On morphologic assessment, palmitate increases HIMC cell number, but cell size and shape remained stable (Supplementary Figure 3*D*). Given the striking effect of long-chain FFAs on HIMC proliferation, we tested medium-chain (decanoate, 10:0) and short-chain (butyrate, 4:0) saturated FFAs, both of which did not increase HIMC proliferation (Supplementary Figure 3*E*), indicating that the HIMC response may be confined to long-chain FFAs. To enhance rigor, we confirmed the effect of palmitate on HIMC proliferation using 2 additional methods: 5-ethynyl-2′-deoxyuridine incorporation and cell counting (Figure 3*E*). Increase in proliferation after exposure to palmitate occurred in HIMCs derived from NL, UC, CDns, and CDs patients in comparable fold changes (Figure 3*F*). This provides a direct link between FFAs released by creeping fat and HIMC proliferation.

Next-Generation Sequencing of Human Intestinal Muscle Cells Exposed to Free Fatty Acids of Different Chain Length Points to Fatty Acid Transport as a Potential Mechanism for the Palmitate-Induced Human Intestinal Muscle Cell Proliferation

To generate hypotheses for later validation of potential pathways for palmitate-induced HIMC proliferation, we treated HIMCs with palmitate or bovine serum albumin (control), followed by next-generation RNA sequencing.[11] Overall gene expression changes in response to all FFAs were modest. One hundred and twenty genes were up-regulated, and 240 genes were down-regulated, considering a fold-change of 1.1 (Figure 4*A*). Top 10 up-regulated genes were PDK4, HOXA-AS3, MIR570, ANGPTL4, PLIN2, CPT1A, PRKG2, MAP2K4P1, CD200, and LOC652276 (Figure 4*A*). Gene Ontology gene set enrichment analysis in palmitate-treated cells revealed ion, adenosine triphosphate, and DNA binding and cell adhesion among the top 10 up-regulated pathways and protein targeting to endoplasmic reticulum, protein targeting to membrane or mitochondrial protein complex among the top 10 down-regulated pathways (Supplementary Table 5*A* and *B*). We next assessed differentially expressed genes and pathways in NL HIMCs exposed to palmitate (long-chain FFA), decanoate (medium-chain FFA), or butyrate (short-chain FFA) by RNA sequencing and compared them with bovine serum albumin (control). Two hundred sixty-five unique genes were up-regulated by palmitate (Figure 4*B*). Gene Ontology pathways pointed toward long-chain FFA transport, lipid metabolism, and FA oxidation as putative signaling events unique to palmitate, but not decanoate- or butyrate-treated HIMCs (Supplementary Table 5*C*).

CD36 and Long-Chain Fatty Acyl CoA Synthetase Are Critical for Palmitate-Induced Human Intestinal Muscle Cell Proliferation

Blockade of the FA translocase CD36, an integral membrane transporter importing FAs into the cell, using sulfo-N-succinimidyl oleate, markedly decreased the proliferative response of HIMC to palmitate (Figure 4*C*). Long-chain FAs are metabolized via long-chain FA acyl-CoA synthetase into FA acyl-CoA.[18] Inhibition of long-chain FA acyl-CoA synthetase in HIMCs by Triascin C numerically reduced baseline HIMC proliferation, but entirely blocked the palmitate-induced proliferative response (Figure 4*D*).

Carnitine Palmitoyltransferase 1A Is Involved in Palmitate-Induced Human Intestinal Muscle Cell Proliferation

CPT-1A, CPT-1B, CPT-1C, and CPT-2 are mitochondrial enzymes with cell type– and tissue-specific distribution, responsible for transport of long-chain FAs into the mitochondria.[19] In the intestinal MP, CPT-1A had the highest gene expression, followed by CPT-2, with the lowest expression detected for CPT-1B and CPT-1C (Figure 4*E*). Immunohistochemistry staining of full-thickness bowel resection tissues showed an increase in CPT-1A–positive cells in the MP of CDs tissue compared with CDns, UC, and NL (Figure 4*F*). In HIMCs derived from different patients with inflammatory bowel disease and NL patients, baseline CPT-1A gene expression was the highest, followed by CPT-2 expression, and CPT-1A gene expression was further increased after treatment of HIMCs with palmitate, but not

Figure 2. Inducible genetic deletion of fat reduces MP thickness in DSS colitis. (*A*) FAT-ATTAC mice or WT mice were subjected to administration of the dimerizer AP20187 twice weekly. Deletion of fat was determined measuring whole-body fat mass via EchoMRI with maximal fat deletion observed starting at week 2. (*B*) *Representative images* of mice euthanized 2 weeks after fat deletion are shown. Presence of abdominal fat in WT-treated animals is marked with *red arrows*. Absence of fat in FAT-ATTAC dimerizer-treated animals is marked with *yellow arrow*. (*C*) Experimental diagram for the DSS colitis model. FAT-ATTAC or WT mice were subjected to administration of the dimerizer AP20187 or vehicle twice weekly starting 2 weeks before 1.5% DSS administration and all throughout the experiment (n = 7–15 per group). (*D*) The severity of DSS-induced colitis was evaluated by measuring the body weight loss. (*E*) Colonic sections were fixed and stained with hematoxylin and eosin for histologic examination. Representative images are shown. *Scale bar:* 100 μm. (*F*) Colonic inflammation score was determined using hematoxylin and eosin sections scored by an inflammatory bowel disease (IBD) pathologist blinded to the experimental groups. (*G*) The severity of fibrosis was evaluated by an IBD pathologist blinded to the experimental groups using Masson trichrome stains. (*H*) Thickness of the colonic MP was measured separately for MP underlying mesenteric fat and the MP not underlying mesenteric fat. Measurements were performed by QuPath software. (*I*) Immunofluorescence for determination of percent cells positive for proliferation marker Ki67 in the colonic MP underlying mesenteric fat with a selective antibody to Ki67 (*red*), desmin (*green*) and 4′,6-diamidino-2-phenylindole (DAPI) (*blue*). *Scale bar:* 20μm. Representative Ki67$^+$ cells are marked with *yellow arrows*. Quantification in *bar graph*. (*J*) Percent positive muscle cells (desmin) that also express the proliferation marker Ki67 indicating the majority of Ki67$^+$ cells being MP smooth muscle cells (n = 5). (*K*) Gene expression of inflammation and fibrosis genes in intestinal tissues relative to 18S ribosomal RNA (n = 6–12). AP20187 is a FK1012 analog. Data are presented as mean ± SEM. *$P < .05$; **$P < .01$; ***$P < .001$.

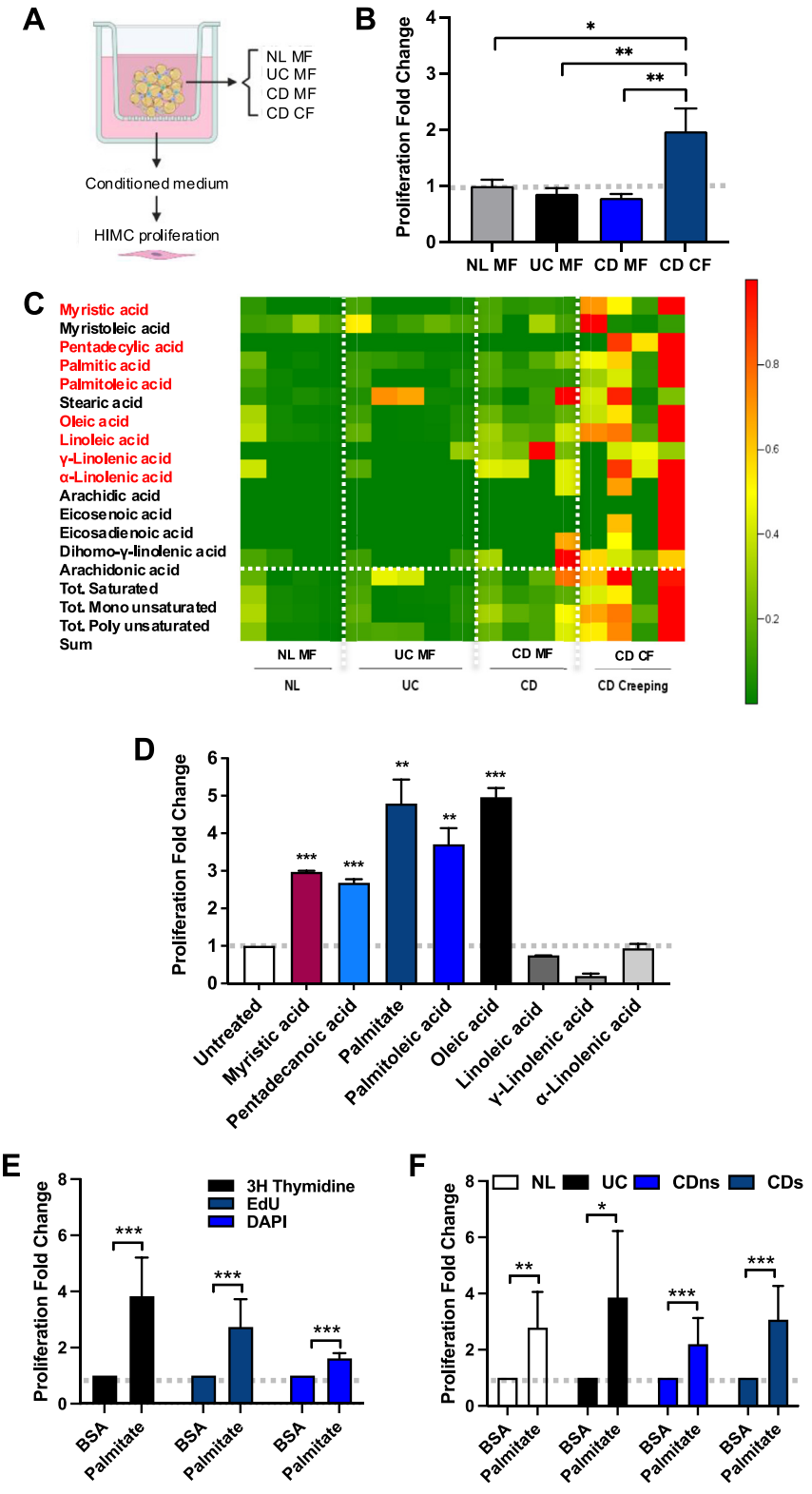

Figure 3. Creeping fat (CF)–derived FAs induce proliferation of primary human intestinal MP smooth muscle cells. (*A*) Experimental diagram for generation of conditioned medium by culture of non-creeping mesenteric fat (MF) from NL, UC, CD, and CD CF, their collection, and use in an HIMC proliferation assay for 48 hours. (*B*) CD CF–conditioned medium induces muscle cell proliferation. Proliferation measured using 3H-thymidine. n = 4–6 per group. (*C*) *Heatmap* of lipidomic analysis of CF and MF derived from NL, UC, CDns, and CDs. FFA significantly elevated in CD CF are colored in *red*. n = 4–5 per group. (*D*) HIMC proliferation after exposure to 50 μM of different FFAs for 48 hours as measured by 3H-thymidine proliferation assay. n = 3 biologic replicates per group, except data for linoleic acid and oleic acid are technical replicates shown from 1 HIMC line. (*E*) HIMC proliferation after exposure to 50 μM palmitate for 48 hours as measured by 3H-thymidine assay, 5-ethynyl-2′-deoxyuridine (EdU) assay and 4′,6-diamidino-2-phenylindole (DAPI) nuclear count. n = 25–28 per group. (*F*) Proliferation of HIMCs derived from NL, UC, CDns, and CDs with or without 50 μM palmitate for 48 hours as measured by EdU assay. n = 5–10 per group. BSA, bovine serum albumin; LCFA, long-chain fatty acid; MCFA, medium-chain fatty acid; SCFA, short-chain fatty acid; Tot., total. Data are presented as mean ± SEM. **P* < .05***P* < .01; ****P* < .001.

decanoate or butyrate (Supplementary Figure 4*A*). CPT-1A knockdown (Supplementary Figure 4*B*) did not affect HIMC baseline proliferation rate, but reduced palmitate-induced HIMC proliferation almost to baseline levels (Figure 4*G*). The small molecule CPT-1 inhibitor etomoxir showed comparable effects (Figure 4*H*). Etomoxir-inhibited palmitate induced HIMC proliferation in HIMCs derived from all tested phenotypes (NL, UC, CDns, and CDs; Supplementary Figure 4*C*). All other long-chain FFAs secreted by creeping fat in increased amounts that also

induced HIMC proliferation (myristic acid, pentadecanoic acid, palmitoleic acid, and oleic acid) also failed to increase HIMC proliferation in the presence of etomoxir (Figure 4*I*).

Our RNA sequencing dataset indicated FA oxidation pathways to be regulated by palmitate and cellular ROS has been linked to increases in cell proliferation.[20] Palmitate increased total

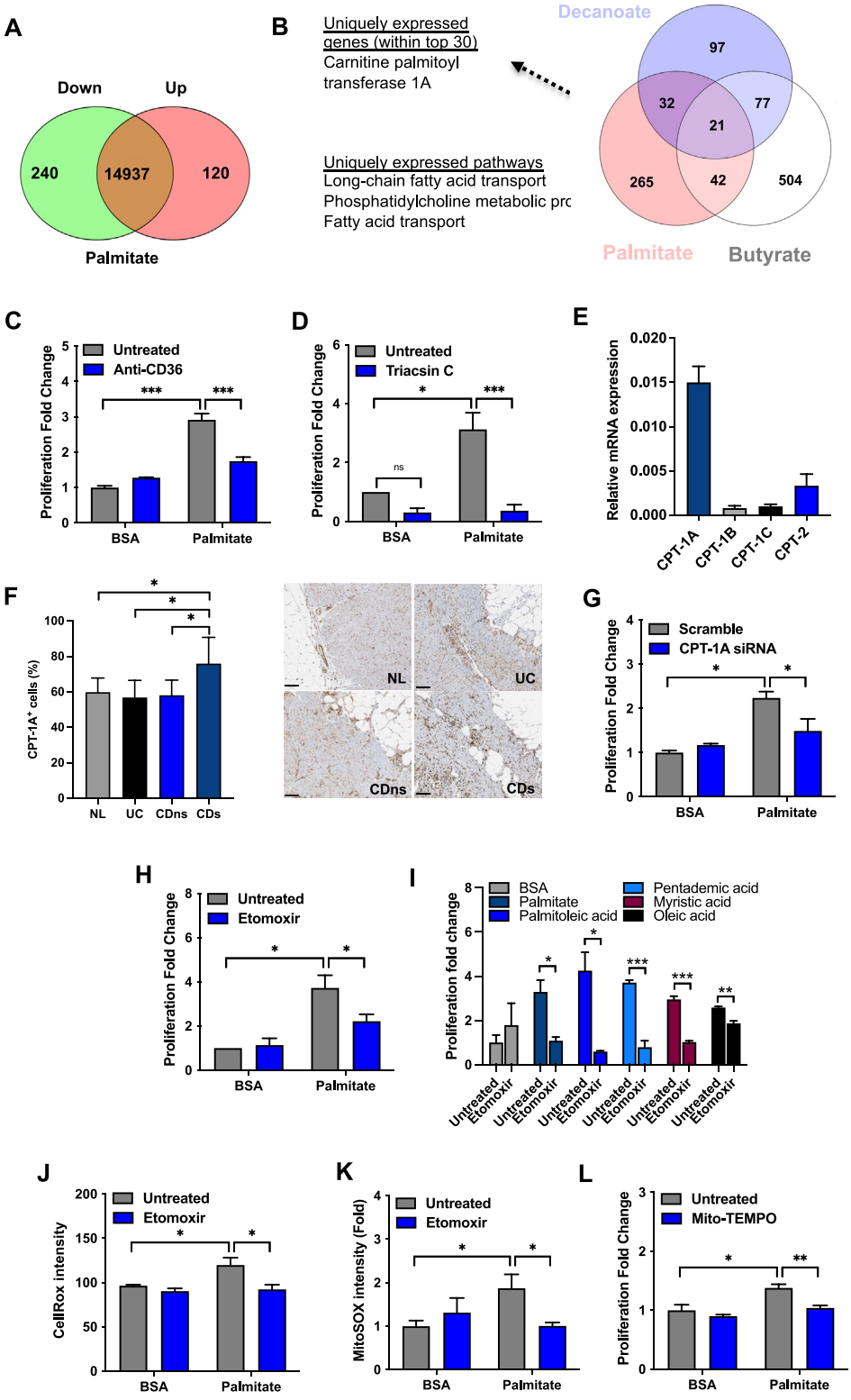

ROS (Figure 4*J*), as well as mitochondrial ROS (Figure 4*K*) in HIMC, which was dependent on CPT-1A, as shown by small interfering RNA knockdown and administration of etomoxir (Supplementary Figure 4*D*). Scavenging ROS through mito-TEMPO–inhibited palmitate induced HIMC proliferation (Figure 4*L*). Data indicate that long-chain FFAs induce HIMC proliferation through FA uptake into mitochondria via CPT-1A and ROS generation.

Metabolic Fate Tracing of Palmitate in Human Intestinal Muscle Cell Reveals Its Conversion Into Phosphatidyl Choline

Exogenous FFAs, such as palmitate, can be an important source of membrane lipids in proliferating cells such as fibroblasts.[21] Exogenous ^{3}H-labeled palmitate, assessed by 1-dimensional thin layer chromatography, was rapidly converted into PLs, triglycerides, and cholesteryl esters, with PL being the major lipid species (Figure 5*A*). A modest fraction of palmitate was converted into FFAs. ^{14}C-acetic acid exposure indicated minimal de novo synthesis of PLs, triglycerides, cholesteryl esters. and FAs in HIMCs, suggesting that the majority of the PLs are metabolically derived from exogenous palmitate (Supplementary Figure 5*A*). Tracing of ^{3}H-palmitate esterification incorporation revealed abundant incorporation into phosphatidyl choline (PC) (Figure 5*B*). Liquid chromatography tandem mass spectrometry lipidomic analysis of HIMCs exposed to deuterium-labeled palmitate revealed PC and phosphatidylserine as major glycerophospholipids containing the deuterated label (Figure 5*C*, *top panel*). Ranking of all fatty acyl esters across all PLs revealed PC and phosphatidylserine subtypes to be the top 5 highest-abundance PLs (18:0/16:0, 16:0/16:0, 16:0/18:1, and 16:0/16:1; Figure 5*C*, *middle* and *low panel*). Pathway analysis revealed that networks related to PC biosynthesis are enriched by these metabolites. Metabolite set enrichment also revealed PL biosynthesis as the most enriched sets (Supplementary Figure 5*B*). Interestingly, blockade of the CDP–choline pathway using small molecule inhibitors of glycerol 3-phosphate acyltransferase did not alter the palmitate-induced HIMC proliferation (Figure 5*D*). In contrast, inhibiting the rate-limiting step in the classic Kennedy pathway through the choline kinase α inhibitor RSM-932A or CTP:choline-phosphate cytidylyltransferase inhibitor CT-2584, blunted palmitate induced HIMC proliferation (Figure 5*E* and *F*). This indicates that palmitate metabolism through the classic Kennedy pathway is involved in palmitate-induced HIMC proliferation (Figure 5*G*).

Blockade of Free Fatty Acid Transport and Metabolism in Human Intestinal Muscle Cells Inhibits Proliferation Induced by Creeping Fat–Conditioned Medium

Next, HIMCs were directly exposed to creeping fat– and CD noncreeping mesenteric fat–conditioned medium. Creeping fat–conditioned medium again induced proliferation of HIMCs and this response was inhibited by blocking CD36, long-chain acetyl-CoA synthetase or CPT-1A (Figure 6*A*). Antioxidant mito-TEMPO inhibited creeping fat–induced HIMC proliferation (Figure 6*B*). Upon inhibition of choline kinase α or CTP:choline-phosphate cytidylyltransferase, creeping fat–induced HIMC proliferation was also blocked (Figure 6*C*). These data support direct relevance of these pathways in the interaction of human creeping fat with the human intestinal MP (Figure 6*D*).

Administration of Carnitine Palmitoyltransferase-1 Inhibitor Etomoxir in Dextran Sodium Sulfate Colitis

We finally sought evidence for the role of CPT-1A in HIMC proliferation in vivo. CPT-1 inhibitor etomoxir was administered intraperitoneally daily in a preventive fashion

Figure 4. Palmitate induces primary human intestinal muscularis propria smooth muscle cell proliferation via FA metabolism and uptake into mitochondria. (*A*) Next-generation sequencing was performed in HIMCs treated with 50 μM palmitate, or control medium for 12 hours (n = 8 per group). *Venn diagram* for up- and down-regulated genes. (*B*) Next-generation sequencing was performed in HIMCs treated with 50 μM palmitate, decanoate, butyrate, or control medium for 12 hours (n = 8 per group). Uniquely changed genes for each FA underwent Gene Ontology pathway analysis and examples of top 10 pathways and genes unique to palmitate are shown. (*C*) HIMC proliferation in response to 50 μM palmitate with or without addition of CD36 inhibitor Sulfosuccinimidyl oleate (SSO) (50 μM) for 48 hours. Proliferation was measured using 3H-thymidine. n = 3. (*D*) HIMC proliferation in response to 50 μM palmitate with or without addition of the long-chain acetyl-CoA synthetase (ACSL) inhibitor Triascin C (10 μM) for 48 hours. Proliferation was measured using 3H-thymidine. n = 3. (*E*) CPT-1A, CPT-1B, CPT-1C, and CPT-2 gene expression in the MP of human intestinal tissues relative to glyceraldehyde 3-phosphate dehydrogenase. n = 7 per group. (*F*) Immunohistochemistry of CPT-1A expression in the MP of human intestinal resection tissues of NL, UC, CDns, and CDs. Quantification of CPT-1A–positive cells relative to all cells using QuPath are shown. *Scale bar:* 100 μm. n = 6–7. (*G*) HIMC proliferation in response to 50 μM palmitate with or without selective small interfering RNA knockdown of CPT-1A for 48 hours. Proliferation was measured using 3H-thymidine. n = 3. (*H*) HIMC proliferation in response to 50 μM palmitate with or without addition of the CPT-1 inhibitor etomoxir (50 μM) for 48 hours. Proliferation was measured using 3H-thymidine. n = 4. (*I*) HIMC proliferation in response to 50 μM of different long-chain FFAs with or without addition of etomoxir (50 μM) for 48 hours. Proliferation was measured using 5-ethynyl-2′-deoxyuridine (EdU) assay. n = 3. (*J*) HIMC ROS production in response to 50 μM palmitate with or without addition of the CPT-1 inhibitor etomoxir (50 μM) for 24 hours. ROS was measured using CellROX Green Reagent. n = 4. (*K*) Mitochondrial ROS production in response to 50 μM palmitate with or without addition of the CPT-1 inhibitor etomoxir (50 μM) for 24 hours were determined in HIMC. ROS was measured using MitoSox. n = 4 technical replicates for 1 HIMC line. (*L*) HIMC proliferation in response to 50 μM palmitate with or without addition of mitochondria-targeted antioxidant mito-TEMPO (10 μM) for 48 hours. Proliferation was measured using EdU. n = 5. Data are presented as mean ± SEM. $^{*}P < .05$; $^{**}P < .01$; $^{***}P < .001$.

in DSS colitis (Figure 7*A*). Etomoxir did not affect DSS-induced weight loss (Figure 7*B*), and showed a marginal reduction in clinical score in DSS-treated mice (Supplementary Figure 6*A* and 6*B*). No difference in colon length was observed when comparing DSS vehicle with DSS etomoxir mice (Supplementary Figure 6*C*). Histologic evaluation for inflammation or fibrosis revealed no difference when comparing DSS vehicle mice with DSS etomoxir mice (Figure 7*C*–*E*). Etomoxir reduced thickness in both the MP underlying mesenteric fat and MP not underlying mesenteric fat compared with vehicle control in the DSS-treated mice (Figure 7*F*, Supplementary Figure 6*D*). In DSS

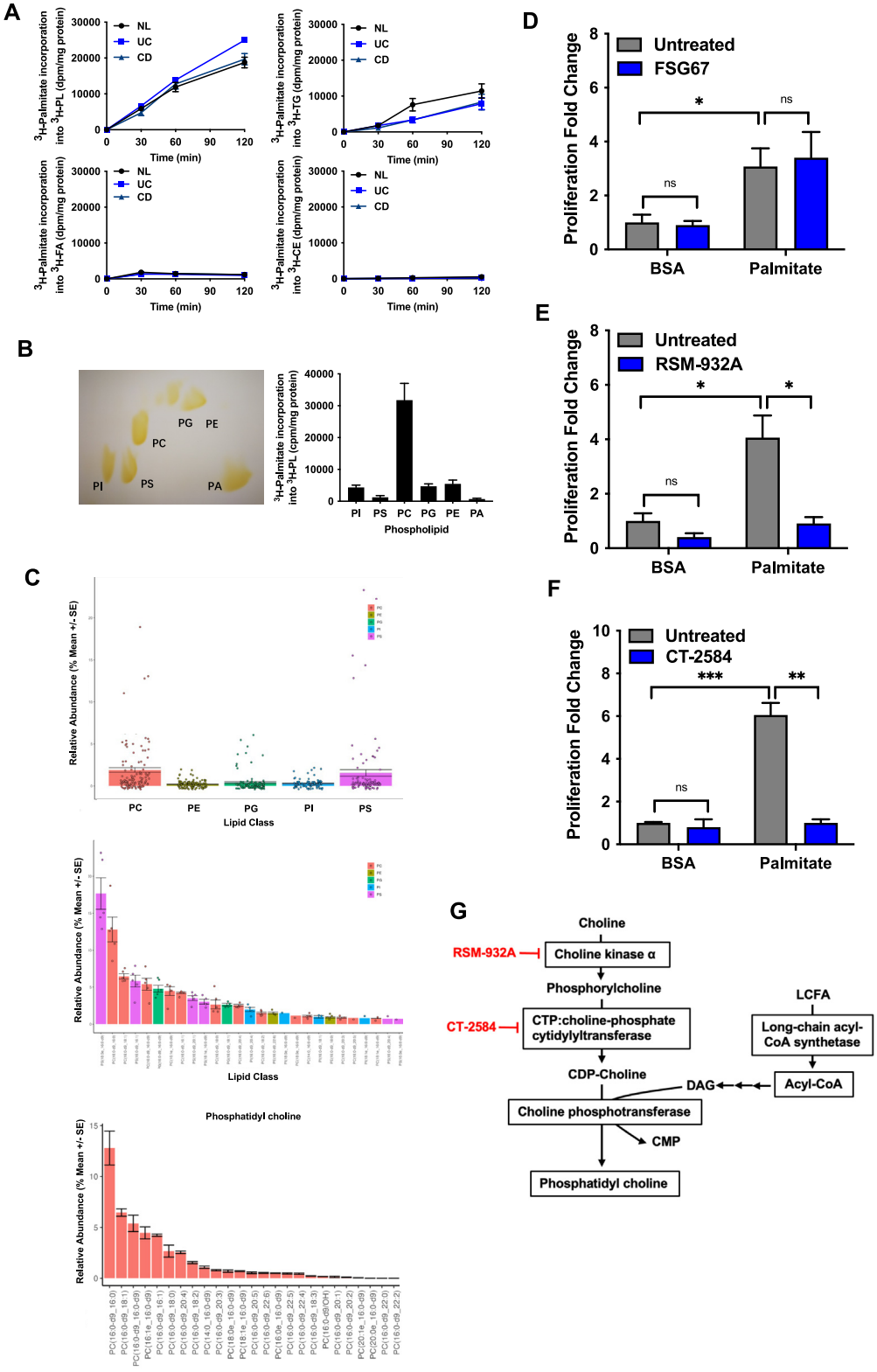

mice treated with etomoxir, the percentage of $Ki67^+$ cells was reduced compared with DSS mice that only received vehicle control (Figure 7*G*). The majority of the $Ki67^+$ cells also stained positive for desmin (Figure 7*H*). There was no difference in inflammatory gene expression in DSS mice regardless of etomoxir administration (Figure 7*I*), indicating that inhibition of CPT-1A reduced muscle proliferation and thickness without affecting inflammation.

Discussion

The role of creeping fat in CD in general and, in particular, its association with the phenotype of stricturing CD, is just starting to be explored. This is striking, as more than three-quarters of bowel segments affected by creeping fat harbor a stricture.[22] In our own resection tissues, we were, in fact, not able to identify a single specimen with stricturing disease that was not surrounded by creeping fat and creeping fat "creeps" underneath the serosal layer and directly on to the MP. This feature is unique and can perhaps only be found in epicardial fat in association with atrial fibrillation,[23] or perivascular fat and atherosclerosis.[24]

Although most studies in the field of stricturing disease focus on the excessive deposition of ECM in the intestinal wall as the major culprit for clinical symptoms in patients with stricturing CD,[1] Chen and colleagues[4] elegantly described that, in fact, a thickening of the MP is the strongest contributor to luminal narrowing and hence symptoms of obstruction in our stricture patients. We confirmed the marked thickening of the MP in patients with stricturing phenotype in our study, but added that once creeping fat was present, the MP showed the largest thickness, as well as an increase in muscle cell proliferation, underscoring the relevance of a potential interaction of the fat with the muscle compartment.

The function of fat is determined by its dynamic and complex composition of distinct cell types, such as immune cells, fibroblasts, among others, with adipocytes, which are rich in lipid droplets, accounting for >90% of the fat volume.[12] Creeping fat contains ample proinflammatory cytokines and is metabolically active, for instance, secreting large amounts of adipokines. Creeping fat is a major source of tumor necrosis factor.[6] It was previously unclear whether and which type of FFAs are released by creeping fat and how those factors affect adjacent tissue layers. Our novel transgenic loss-of-fat animal model, established that the absence of mesenteric adipocytes prevents MP thickening in response to inflammation, suggesting that the adipocytes are a requirement for the proliferative MP response seen in humans.[4] This was confirmed by coculture of human creeping fat–conditioned medium with HIMC. Using lipidomics as an unbiased approach, we identified several FFAs, predominantly palmitate, to be released by creeping fat, suggesting active lipolysis, perhaps induced by proinflammatory mediators, such as tumor necrosis factor, within the creeping fat.[6] This also corroborates recent lipidomics analysis of patients with CD and healthy controls, which revealed abnormal lipid metabolism in creeping fat.[25] Those FFAs induced a very robust increase in HIMC proliferation, in fact, stronger than any previously reported cytokines or growth factors in in vitro systems using intestinal fibroblasts or HIMCs. Palmitate and other long-chain FFAs inducing proliferation have previously been reported in colorectal cancer cells,[26] but not in intestinal smooth muscle cells or in smooth muscle cells in general. Although our studies suggest a direct effect of FFAs on muscle proliferation and that FFAs may be required for the MP to thicken, we cannot exclude other factors driving muscle proliferation. In fact, we believe that multiple mediators expressed in the intestinal mucosa, submucosa, MP, or fat have the potential to induce smooth muscle hyperplasia, and this is part of future investigations.

What remained to be determined were mechanisms of FFA-induced proliferation. With guidance of next-generation sequencing of HIMCs exposed to FFAs of different chain length, we identified FA transport and metabolism as a putative mechanism. This hypothesis was strengthened by data from other cell types, such as nasopharyngeal carcinoma cells[27] and breast cancer cells,[28] suggesting palmitate signaling driving proliferation through intracellular metabolism, uptake into mitochondria, and ultimately undergoing beta oxidation. In fact, we were able to show

Figure 5. Palmitate induces proliferation of primary HIMCs via FA metabolism. (*A*) HIMCs derived from NL, UC, or CD tissues were exposed to ^{3}H-labeled palmitate for 30, 60, and 120 minutes and lipids contained in HIMCs were extracted using chloroform/methanol. The extracted lipids were separated and the incorporation of ^{3}H-palmitate into PLs, cholesteryl ester (CE), triglyceride (TG), and FFA was determined by the radioactivity quantified by liquid scintillation counting. n = 4. (*B*) PL analysis was performed using 2-dimensional thin-layer chromatography with *yellow spots* corresponding to labeled lipids, including phosphatidylethanolamine (PE), PC, phosphatidic acid (PA), phosphatidylglycerol (PG), phosphatidylserine (PS), and phosphatidylinositol (PI). Representative chromatography depicted on *left* and quantification using liquid scintillation counting depicted on *right*. n = 3. (*C*) HIMCs were exposed to 50 μM deuterium–labeled palmitate for 1 hour, followed by lipidomic analysis. *Top panel* indicates relative abundance of the deuterated label by lipid class. *Middle panel* indicates relative abundance of the deuterated label ranked by individual lipids across lipid classes. *Low panel* indicates relative abundance of the deuterated label ranked by individual lipids within the PC class. (*D*) HIMC proliferation in response to 50 μM palmitate with or without addition of the glycerol 3-phosphate acyltransferase (GPAT) inhibitor FSG67 (200 μM) for 48 hours. Proliferation was measured using 5-ethynyl-2′-deoxyuridine (EdU) assay. n = 3. (*E*) HIMC proliferation in response to 50 μM PA with or without addition of the choline kinase α inhibitor RSM-932A (20 μM) for 48 hours. Proliferation was measured using EdU assay. n = 3. (*F*) HIMC proliferation in response to 50 μM palmitate with or without addition of the CTP:choline-phosphate cytidylyltransferase inhibitor CT-2584 (2.5 μM) for 48 hours. Proliferation was measured using EdU assay. n = 3. (*G*) *Diagram* depicting the discovered choline synthesis pathways in HIMC. Small molecule inhibitors are depicted in *red*. BSA, bovine serum albumin; DAG, diacylglycerol; LFCA, long-chain fatty acid.

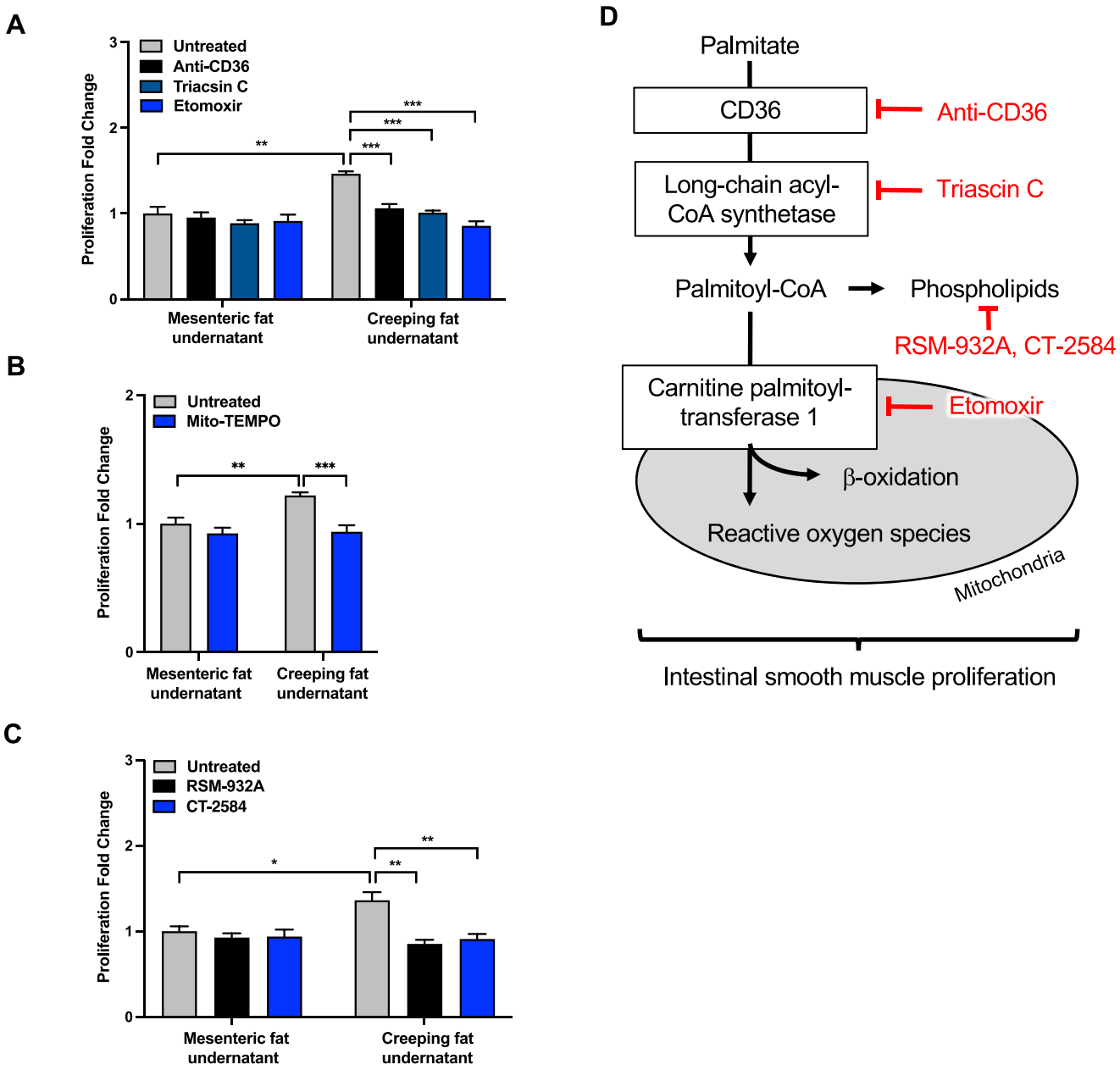

Figure 6. Creeping fat (CF)– and noncreeping mesenteric fat (MF)–conditioned medium induces proliferation of primary HIMCs via CPT-1 and FA metabolism. (*A*) Cell culture medium was conditioned for 48 hours using 50 mg wet weight of CF or noncreeping MF from CD. Subsequently, conditioned medium was cocultured with HIMCs with or without the presence of the CD36 inhibitor sulfosuccinimidyl oleate (50 μM), the CPT-1 inhibitor etomoxir (50 μM), or the long-chain acetyl-CoA synthetase inhibitor Triascin C (10 μM) for 48 hours and proliferation measured using 5-ethynyl-2′-deoxyuridine (EdU) for 48 hours. n = 4 per group. (*B*) HIMCs were co-cultured with cell culture medium–conditioned from CF or noncreeping MF of CD with or without the presence of mitochondria-targeted antioxidant mito-TEMPO (10 μM) for 48 hours and proliferation measured using EdU assay. n = 4 per group. (*C*) HIMCs were cocultured with cell culture medium conditioned from CF or noncreeping MF of CD with or without the presence of the choline kinase α inhibitor RSM-932A (20 μM) or the CTP:choline-phosphate cytidylyltransferase inhibitor CT-2584 (2.5 μM) for 48 hours and proliferation measured using EdU assay. n = 4 per group. (*D*) *Diagram* depicting the discovered signaling pathways in HIMC. Small molecule inhibitors are depicted in *red*.

conclusively, with a combination of in vitro and in vivo studies, that palmitate and other long-chain FFAs are using CPT-1A to enter mitochondria and increase ROS, and that proliferation of HIMCs was dependent on those steps.

For cells to divide, an expansion of the cellular membrane is required, which makes a larger pool of PLs necessary. As an additional mechanism on how palmitate, and perhaps other FFAs, could enhance proliferation, we identified that palmitate is predominantly metabolized into PC. PC is synthesized in cells via the choline metabolism pathways and the first step in the synthesis of PC is the phosphorylation of choline via choline kinase α to form

phosphocholine. In the second step, CMP is transferred from CTP to phosphocholine to form CDP-choline by the rate-limiting enzyme CTP:phosphocholine cytidylyltransferase.[29] In our experimental system, the choline kinase α inhibitor RSM-932A or the CTP:choline-phosphate cytidylyltransferase inhibitor CT-2584 inhibited the palmitate-induced HIMC proliferation, indicating that CDP–choline pathway may be involved in palmitate-induced HIMC proliferation. Because inhibition of either the CPT-1A pathway or the choline pathway was able to completely abrogate the palmitate-induced HIMC proliferation, one may speculate that both are required to accomplish the increase cell division needed by HIMCs to thicken the MP.

Finally, and most importantly, when directly exposing HIMCs to creeping fat–conditioned medium in vitro with

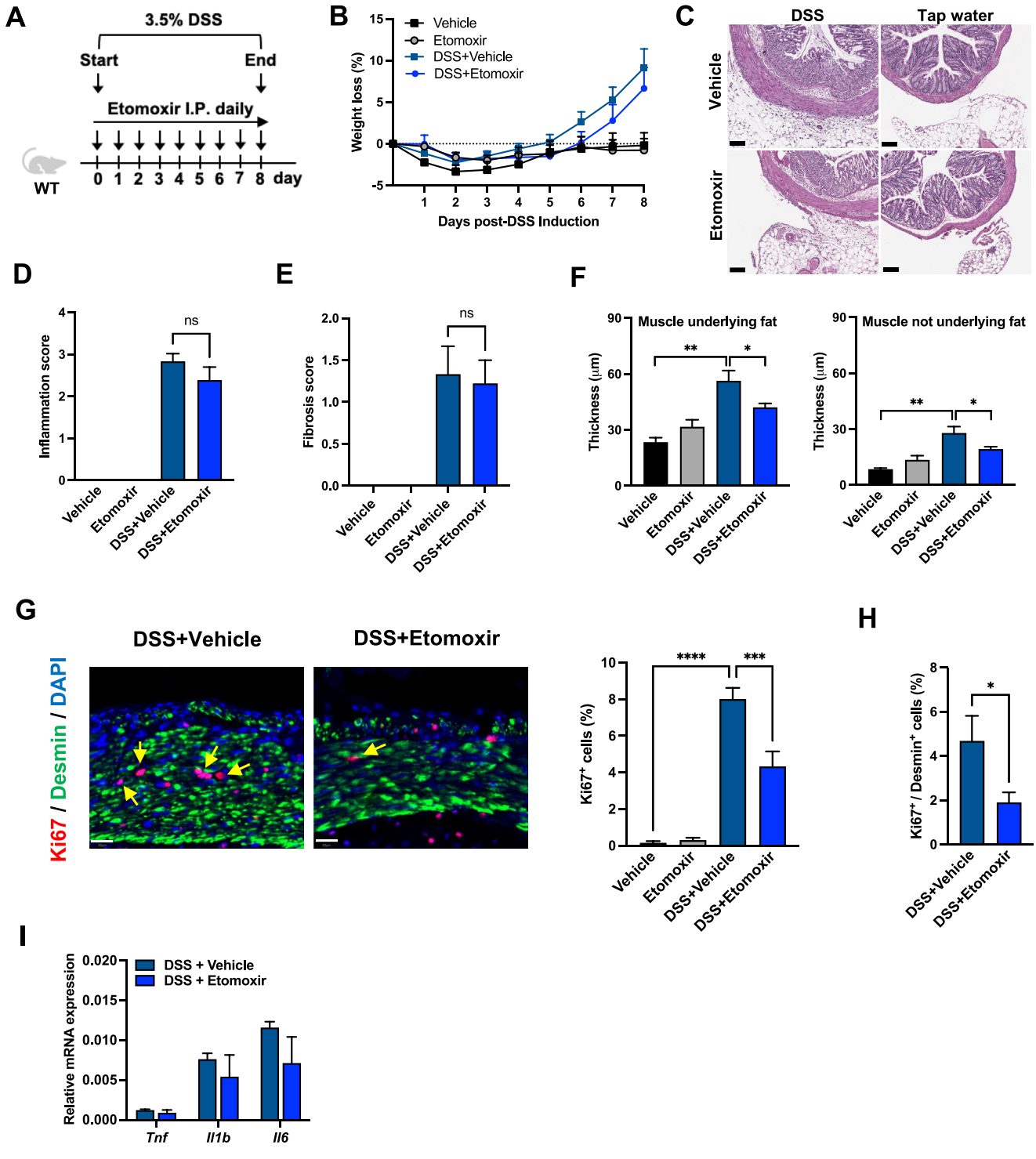

and without blockade of CPT-1A and choline metabolism inhibitors, we confirmed the identified mechanistic pathways in a human tissue compartment interaction model, and inhibition of CPT-1A, in fact, prevents muscle thickening in experimental colitis.

Our study has multiple strengths. To our knowledge, this is the first investigation providing a direct functional link of creeping fat with the muscle thickness in stricturing CD. We provide a truly translational approach with primary human cells and tissues, as well as a novel transgenic loss-of-function animal model. CPT-1A has not been investigated in relation to intestinal inflammation or strictures. Strikingly, the effect of CPT-1A appeared to affect muscle proliferation, but not inflammation or the expression of ECM in our model systems. There are also some limitations to our work. Although several animal models for creeping fat have been described,[30,31] we believe they do not sufficiently reflect the human phenomenon, and that a loss-of-function approach was better suited to confirm our hypothesis. To establish the interaction of FA and the MP in experimental colitis, we purposefully chose acute colitis models only, as the MP thickness in this setting is prominent and modifiable. Future studies will examine additional acute and chronic colitis models with prevention and reversal of MP thickening, which was considered out of scope for this already substantial dataset. At that time, we will examine whether CPT-1A modulation in fibroblasts in dedicated fibrosis animal models will show an impact on ECM production. The reduction of fat in the FAT-ATTAC mouse is not restricted to the mesenteric fat, but involves fat reduction in the entire mouse body. We cannot exclude that fat loss in other compartments could influence MP thickness in the gut. Due to the limitations of human tissue procurement, we used a combination of paired, strictured, and nonstrictured segments derived from the same patient with CD, as well as individual segments from CD stricture or nonstricture subjects. This is because we required the co-presence of noncreeping mesenteric/creeping fat and MP and well-oriented and present tissue layers in each segment. Due to same restrictions, the number of samples for the lipidomics experiments is modest and, hence, we put a strong emphasis on a thorough functional validation of the results. We were not able to control our experiments with noncreeping mesenteric fat derived from segments with stricturing CD, as all our stricture segments exhibited creeping fat. This is consistent with the literature and identical findings have been reported previously.[17,32] It remains to be determined whether and how creeping fat influences intestinal fibrosis and inflammation, as our work focused on the contribution of FFAs to disease. Future work needs to elucidate further whether creeping fat represents a protective response or is an initiator and perpetuator of CD or both.

A significant therapeutic implication of this study is the provision of a mechanistic proof of principle that the effect of creeping fat on the MP can be pharmacologically inhibited. Etomoxir was able to block FFA-induced proliferation and was previously tested in clinical development programs for chronic heart failure.[33] Concerns about hepatotoxic effects of etomoxir hampered the ultimate use in patients, but more selective, more potent small molecules or local delivery formulations, may make this approach more feasible for future use in patients with CD strictures. Through the work of the Stenosis Therapy and Anti-Stricture Research Consortium, clinical trials for stricturing disease have now begun (ClinicalTrials.gov, Number NCT05843578 for STENOVA). Clinical trial end points have been developed and continue to be refined, providing hope to our patients with stricturing CD. Selective inhibition of muscle thickening in stricturing CD has to date not been tested and we wish our work will put spotlight on this understudied problem.

Supplementary Material

Note: To access the supplementary material accompanying this article, visit the online version of *Gastroenterology* at www.gastrojournal.org, and at https://doi.org/10.1053/j.gastro.2024.10.034.

References

1. Rieder F, Mukherjee PK, Massey WJ, et al. Fibrosis in IBD: from pathogenesis to therapeutic targets. Gut 2024; 73:854–866.
2. Lin S, Wang J, Mukherjee PK, et al. Milk fat globule-epidermal growth factor 8 (MFGE8) prevents intestinal fibrosis. Gut 2024;73:1110–1123.

Figure 7. Administration of the CPT inhibitor etomoxir reduces MP thickness, but not inflammation or fibrosis in DSS colitis. (*A*) Experimental diagram for the DSS colitis model. Balb/c WT mice were subjected to administration of etomoxir or vehicle intraperitoneally (I.P.) daily starting the day of 3.5% DSS administration and all throughout the experiment. (*B*) The severity of DSS-induced colitis was evaluated by measuring the body weight loss (n = 5–9 per group). (*C*) Colonic sections were fixed and stained with hematoxylin and eosin for histologic examination. *Representative images* are shown. *Scale bar:* 100 μm. (*D*) Colonic inflammation score was determined using hematoxylin and eosin sections scored by an inflammatory bowel disease (IBD) pathologist blinded to the experimental groups (n = 5–9 per group). (*E*) The severity of fibrosis was evaluated by an IBD pathologist blinded to the experimental groups using Masson trichrome staining (n = 5–9 per group). (*F*) Thickness of the colonic MP was measured separately for MP underlying mesenteric fat and the MP not underlying mesenteric fat (n = 5–9 per group). Measurements were performed by QuPath software. (*G*) Immunofluorescence for determination of percent cells positive for proliferation marker Ki67 in the colonic MP underlying mesenteric fat with a selective antibody to Ki67 (*red*), desmin (*green*), and 4′,6-diamidino-2-phenylindole (DAPI) (*blue*). *Scale bar:* 20 μm. Representative Ki67$^+$ cells are marked with *yellow arrows*. Quantification in *bar graph*. n = 6 per group. *Scale bar:* 20 μm. (*H*) Percent positive muscle cells (desmin) that also express the proliferation marker Ki67, indicating the majority of Ki67$^+$ cells were muscle cells. (*I*) Gene expression of inflammation genes in intestinal tissues relative to 18S ribosomal RNA. n = 5 per group. Data are presented as mean ± SEM. *$P < .05$; **$P < .01$; ***$P < .001$.

3. Mao R, Doyon G, Gordon IO, et al. Activated intestinal muscle cells promote preadipocyte migration: a novel mechanism for creeping fat formation in Crohn's disease. Gut 2022;71:55–67.
4. Chen W, Lu C, Hirota C, et al. Smooth muscle hyperplasia/hypertrophy is the most prominent histological change in Crohn's fibrostenosing bowel strictures: a semiquantitative analysis by using a novel histological grading scheme. J Crohns Colitis 2017;11:92–104.
5. Crohn BB, Ginzburg L, Oppenheimer GD. Regional ileitis; a pathologic and clinical entity. Am J Med 1952;13:583–590.
6. Kredel LI, Siegmund B. Adipose-tissue and intestinal inflammation - visceral obesity and creeping fat. Front Immunol 2014;5:462.
7. Borley NR, Mortensen NJ, Jewell DP, et al. The relationship between inflammatory and serosal connective tissue changes in ileal Crohn's disease: evidence for a possible causative link. J Pathol 2000;190:196–202.
8. Mukherjee PK, Nguyen QT, Li J, et al. Stricturing Crohn's disease single-cell RNA sequencing reveals fibroblast heterogeneity and intercellular interactions. Gastroenterology 2023;165:1180–1196.
9. Rieder F, Georgieva M, Schirbel A, et al. Prostaglandin E2 inhibits migration of colonic lamina propria fibroblasts. Inflamm Bowel Dis 2010;16:1505–1513.
10. Lin SN, Musso A, Wang J, et al. Human intestinal myofibroblasts deposited collagen VI enhances adhesiveness for T cells - a novel mechanism for maintenance of intestinal inflammation. Matrix Biol 2022;113:1–21.
11. Zhao S, Dejanovic D, Yao P, et al. Selective deletion of MyD88 signaling in alpha-SMA positive cells ameliorates experimental intestinal fibrosis via post-transcriptional regulation. Mucosal Immunol 2020;13:665–678.
12. Mao R, Kurada S, Gordon IO, et al. The mesenteric fat and intestinal muscle interface: creeping fat influencing stricture formation in Crohn's disease. Inflamm Bowel Dis 2019;25:421–426.
13. Pajvani UB, Trujillo ME, Combs TP, et al. Fat apoptosis through targeted activation of caspase 8: a new mouse model of inducible and reversible lipoatrophy. Nat Med 2005;11:797–803.
14. Bloom SM, Bijanki VN, Nava GM, et al. Commensal Bacteroides species induce colitis in host-genotype-specific fashion in a mouse model of inflammatory bowel disease. Cell Host Microbe 2011;9:390–403.
15. Bankhead P, Loughrey MB, Fernandez JA, et al. QuPath: open source software for digital pathology image analysis. Sci Rep 2017;7:16878.
16. Bibus D, Lands B. Balancing proportions of competing omega-3 and omega-6 highly unsaturated fatty acids (HUFA) in tissue lipids. Prostaglandins Leukot Essent Fatty Acids 2015;99:19–23.
17. Sheehan AL, Warren BF, Gear MW, et al. Fat-wrapping in Crohn's disease: pathological basis and relevance to surgical practice. Br J Surg 1992;79:955–958.
18. Ellis JM, Bowman CE, Wolfgang MJ. Metabolic and tissue-specific regulation of acyl-CoA metabolism. PLoS One 2015;10:e0116587.
19. Guth A, Monk E, Agarwal R, et al. Targeting fat oxidation in mouse prostate cancer decreases tumor growth and stimulates anti-cancer immunity. Int J Mol Sci 2020;21:9660.
20. Han MJ, Kim BY, Yoon SO, et al. Cell proliferation induced by reactive oxygen species is mediated via mitogen-activated protein kinase in Chinese hamster lung fibroblast (V79) cells. Mol Cells 2003;15:94–101.
21. Yao CH, Fowle-Grider R, Mahieu NG, et al. Exogenous fatty acids are the preferred source of membrane lipids in proliferating fibroblasts. Cell Chem Biol 2016;23:483–493.
22. Coffey JC, O'Leary DP, Kiernan MG, et al. The mesentery in Crohn's disease: friend or foe? Curr Opin Gastroenterol 2016;32:267–273.
23. Thanassoulis G, Massaro JM, O'Donnell CJ, et al. Pericardial fat is associated with prevalent atrial fibrillation: the Framingham Heart Study. Circ Arrhythm Electrophysiol 2010;3:345–350.
24. van Dam AD, Boon MR, Berbee JF, et al. Targeting white, brown and perivascular adipose tissue in atherosclerosis development. Eur J Pharmacol 2017;816:82–92.
25. Wu F, Wu F, Zhou Q, et al. A CCL2(+)DPP4(+) subset of mesenchymal stem cells expedites aberrant formation of creeping fat in humans. Nat Commun 2023;14:5830.
26. Fatima S, Hu X, Huang C, et al. High-fat diet feeding and palmitic acid increase CRC growth in beta2AR-dependent manner. Cell Death Dis 2019;10:711.
27. Tang M, Dong X, Xiao L, et al. CPT1A-mediated fatty acid oxidation promotes cell proliferation via nucleoside metabolism in nasopharyngeal carcinoma. Cell Death Dis 2022;13:331.
28. Jariwala N, Mehta GA, Bhatt V, et al. CPT1A and fatty acid beta-oxidation are essential for tumor cell growth and survival in hormone receptor-positive breast cancer. NAR Cancer 2021;3:zcab035.
29. Henneberry AL, Wright MM, McMaster CR. The major sites of cellular phospholipid synthesis and molecular determinants of fatty acid and lipid head group specificity. Mol Biol Cell 2002;13:3148–3161.
30. Xiong S, Ta-Chiang L, Frank L, et al. Characterization and modeling of the creeping fat that occurs in Crohn's disease. Gastroenterology 2019;156:S–S445.
31. Eichele DD, Kharbanda KK. Dextran sodium sulfate colitis murine model: an indispensable tool for advancing our understanding of inflammatory bowel diseases pathogenesis. World J Gastroenterol 2017;23:6016–6029.
32. Coffey CJ, Kiernan MG, Sahebally SM, et al. Inclusion of the mesentery in ileocolic resection for Crohn's disease is associated with reduced surgical recurrence. J Crohns Colitis 2018;12:1139–1150.
33. Holubarsch CJ, Rohrbach M, Karrasch M, et al. A double-blind randomized multicentre clinical trial to evaluate the efficacy and safety of two doses of etomoxir in comparison with placebo in patients with moderate congestive heart failure: the ERGO (etomoxir for the recovery of glucose oxidation) study. Clin Sci (Lond) 2007;113:205–212.

Received March 25, 2024. Accepted October 16, 2024.

Correspondence
Address correspondence to: Florian Rieder, MD, Department of Gastroenterology, Hepatology and Nutrition, Digestive Diseases Institute, 9500 Euclid Avenue, Cleveland, Ohio 44195. e-mail: riederf@ccf.org.

Acknowledgments
The authors thank Dr Judith Drazba, Dr John Peterson, Andrelie Branicky, and Apryl Helmick from the Lerner Research Institute Microscopy and Image Core, for help in microscopy and image analysis. The authors thank Dr Pieter W. Faber (Director, University of Chicago Genomics Facility) for facilitating RNA sequencing. The authors acknowledge the support of the Departments of Colorectal Surgery and Pathology of the Cleveland Clinic. Tissue samples were provided by the Human Tissue Procurement Facility of the Cleveland Clinic through the services of the Biorepository Core funded by National Institutes of Health grant P30 DK097948.

Weiwei Liu, Ren Mao, and Thi Hong Nga Le contributed equally to this work.

CrediT Authorship Contributions
Weiwei Liu, PhD (Conceptualization: Supporting; Data curation: Lead; Formal analysis: Lead; Investigation: Lead; Methodology: Lead; Writing – original draft: Lead; Writing – review & editing: Lead)

Ren Mao, MD (Data curation: Equal; Formal analysis: Equal; Investigation: Equal)

Thi Hong Nga Le, PhD (Data curation: Equal; Formal analysis: Equal; Investigation: Equal; Methodology: Equal)

Gail West, BS (Data curation: Supporting; Methodology: Supporting; Writing – review & editing: Supporting)

Venkateshwari Varadharajan, PhD (Data curation: Supporting; Methodology: Supporting)

Rakhee Banerjee, PhD (Data curation: Supporting; Methodology: Supporting)

Genevieve Doyon, PhD (Data curation: Supporting; Writing – review & editing: Supporting)

Pranab Mukherjee, PhD (Data curation: Supporting; Formal analysis: Supporting; Methodology: Supporting; Software: Supporting; Writing – review & editing: Supporting)

Quang Tam Nguyen, PhD (Data curation: Supporting; Methodology: Supporting; Writing – review & editing: Supporting)

Anny Mulya, PhD (Data curation: Supporting; Writing – review & editing: Supporting)

Julie H. Rennison, PhD (Data curation: Supporting; Writing – review & editing: Supporting)

Ilyssa O. Gordon, MD (Data curation: Supporting; Writing – review & editing: Supporting)

Michael Cruise, MD, PhD (Data curation: Supporting; Writing – review & editing: Supporting)

Shaomin Hu, MD (Data curation: Supporting; Methodology: Supporting; Writing – review & editing: Supporting)

Doug Czarnecki, HSD (Data curation: Supporting; Methodology: Supporting)

Thomas Plesec, MD (Data curation: Supporting)

Jyotsna Chandra, PhD (Data curation: Supporting; Writing – review & editing: Supporting)

Suhanti Banerjee, MS (Data curation: Supporting; Methodology: Supporting)

Jie Wang, PhD (Data curation: Supporting; Writing – review & editing: Supporting)

William J. Massey, PhD (Data curation: Supporting; Writing – review & editing: Supporting)

Idan Goren, MD (Data curation: Supporting; Writing – review & editing: Supporting)

Si-Nan Lin, MD (Data curation: Supporting; Writing – review & editing: Supporting)

Satya Kurada, MD, MS (Data curation: Supporting; Writing – review & editing: Supporting)

Benjamin L. Cohen, MD (Data curation: Supporting; Writing – review & editing: Supporting)

Taha Qazi, MD (Data curation: Supporting; Writing – review & editing: Supporting)

Stefan D. Holubar, MD (Data curation: Supporting; Writing – review & editing: Supporting)

Jeremy Lipman, MD (Data curation: Supporting; Writing – review & editing: Supporting)

Arielle Kanters, MD (Data curation: Supporting; Writing – review & editing: Supporting)

Christy M. Gliniak, PhD (Data curation: Supporting; Writing – review & editing: Supporting)

Philipp E. Scherer, PhD (Data curation: Supporting; Resources: Supporting; Writing – review & editing: Supporting)

Min-Hu Chen, MD (Data curation: Supporting; Writing – review & editing: Supporting)

Britta Siegmund, MD (Supervision: Supporting; Writing – original draft: Supporting; Writing – review & editing: Supporting)

Andrei I. Ivanov, PhD (Data curation: Supporting; Writing – review & editing: Supporting)

Claudio Fiocchi, MD (Data curation: Supporting; Writing – review & editing: Supporting)

David R. Van Wagoner, PhD (Data curation: Supporting; Writing – review & editing: Supporting)

J. Mark Brown, PhD (Data curation: Supporting; Methodology: Supporting; Writing – review & editing: Supporting)

Florian Rieder, MD (Conceptualization: Lead; Data curation: Lead; Formal analysis: Lead; Funding acquisition: Lead; Investigation: Lead; Methodology: Lead; Project administration: Lead; Resources: Lead; Software: Lead; Supervision: Lead; Writing – original draft: Lead; Writing – review & editing: Lead)

Conflicts of interest
These authors disclose the following: Ilyssa O. Gordon receives research support from Celgene Corporation, Morphic Therapeutics, and Alimentiv. For all: Ilyssa O. Gordon receives no direct funds; Cleveland Clinic receives funds on her behalf. Min-Hu Chen is consultant to Janssen, Takeda, AbbVie, China Medical System, and Ipsen. Satya Kurada is consultant to Bristol Myers Squibb. Benjamin L. Cohen receives the following financial support: advisory boards and consultant for AbbVie, Celgene-Bristol Myers Squibb, Emmes Biopharma Services LLC (DSMB), Lilly, Pfizer, Sublimity Therapeutics, Takeda, TARGET RWE; CME companies: Cornerstones, Vindico; Speaking: AbbVie; Educational Grant: Pfizer. Taha Qazi is a consultant for AbbVie, Celgene/Bristol Myers Squibb, Prometheus Biosciences, and Janssen. Stefan D. Holubar is a consultant to Takeda. Britta Siegmund is a consultant for AbbVie, Arena, Boehringer Ingelheim, Bristol Myers Squibb, Celgene, Eli Lilly, Endpoint Health, Falk Pharma, Galapagos, Gilead, Janssen, Landos, Pfizer, Prometheus, and Takeda; has received speaker fees from AbbVie, CED Service GmbH, Eli Lilly, Falk Pharma, Ferring, Galapagos, Janssen, Novartis, Pfizer, and Takeda. Claudio Fiocchi received speaker fees from UCB, Genentech, Sandoz, and Janssen, and he is consultant for Athos Therapeutics, Inc. Florian Rieder is consultant to Adiso, Adnovate, Agomab, Allergan, AbbVie, Arena, AstraZeneca, Bausch & Lomb, Boehringer-Ingelheim, Celgene/BMS, Celltrion, CDISC, Celsius, Cowen, Eugit, Ferring, Galapagos, Galmed, Genentech, Gilead, Gossamer, Granite, Guidepoint, Helmsley, Horizon Therapeutics, Image Analysis Limited, Index Pharma, Landos, Jannsen, Koutif, Mestag, Metacrine, Mirum, Mopac, Morphic, Myka Labs, Organovo, Origo, Palisade, Pfizer, Pliant, Prometheus Biosciences, Receptos, RedX, Roche, Samsung, Sanofi, Surmodics, Surrozen, Takeda, Techlab, Teva, Theravance, Thetis, Trix Bio, UCB, Ysios, and 89Bio. The remaining authors disclose no conflicts.

Funding
This work was supported by the Helmsley Charitable Trust through the Stenosis Therapy and Anti-Fibrotic Research Consortium (no. 3081), the Crohn's and Colitis Foundation (no. 569125), National Institutes of Health (NIH) National Institute of Diabetes and Digestive and Kidney Diseases (NIDDK) grants R01 123233, R01 132038, and R01 130227, NIH NIDDK grant P30 DK097948 to Claudio Fiocchi, J. Mark Brown, Andrei I. Ivanov, and Florian Rieder, NIH NIDDK grant K01 131252 to Christy M. Gliniak, NIH National Institute on Alcohol Abuse and Alcoholism grant P50 AA024333 to J. Mark Brown, Cleveland Clinic through the LabCo program to Florian Rieder, and National Science Foundation of China (81970483, 82170537, and 82222010) to Ren Mao and the German Research Foundation (CRC-TRR 241-B01 and Z02 (project number 375876048); CRU 5023 (project number 50474582), CRC 1449-B04 and Z02 (project number 431232613); CRC 1340-B06 (project number 372486779) to Britta Siegmund.

Data Availability
The transcriptomic datasets will be shared upon request. Please contact the corresponding author for any inquiries. The Cleveland Clinic agrees to use NIH's Federal Demonstration Partnership Data Use Agreement template to share the data, which can be found at https://thefdp.org/default/committees/research-compliance/data-stewardship/. Any other data, analytic methods, and study materials will be made available to other researchers upon reasonable request.